



<https://doi.org/10.1038/s42003-022-04271-2>

OPEN

Fission yeast Dis1 is an unconventional TOG/XMAP215 that induces microtubule catastrophe to drive chromosome pulling

Yuichi Murase¹, Masahiko Yamagishi ², Naoyuki Okada^{1,3}, Mika Toya ^{1,4,5}, Junichiro Yajima ^{2,6,7}, Takahiro Hamada⁸ & Masamitsu Sato ^{1,5,9} 

The shortening of microtubules attached to kinetochores is the driving force of chromosome movement during cell division. Specific kinesins are believed to shorten microtubules but are dispensable for viability in yeast, implying the existence of additional factors responsible for microtubule shortening. Here, we demonstrate that Dis1, a TOG/XMAP215 ortholog in fission yeast, promotes microtubule shortening to carry chromosomes. Although TOG/XMAP215 orthologs are generally accepted as microtubule polymerases, Dis1 promoted microtubule catastrophe *in vitro* and *in vivo*. Notably, microtubule catastrophe was promoted when the tip was attached to kinetochores, as they steadily anchored Dis1 at the kinetochore-microtubule interface. Engineered Dis1 oligomers artificially tethered at a chromosome arm region induced the shortening of microtubules in contact, frequently pulling the chromosome arm towards spindle poles. This effect was not brought by oligomerised Alp14. Thus, unlike Alp14 and other TOG/XMAP215 orthologs, Dis1 plays an unconventional role in promoting microtubule catastrophe, thereby driving chromosome movement.

¹Laboratory of Cytoskeletal Logistics, Department of Life Science and Medical Bioscience, Graduate School of Advanced Science and Engineering, Waseda University, 2-2 Wakamatsucho, Shinjuku-ku, Tokyo 162-8480, Japan. ²Department of Life Sciences, Graduate School of Arts and Sciences, The University of Tokyo, 3-8-1 Komaba, Meguro-ku 153-8902 Tokyo, Japan. ³Instituto de Biologia Molecular e Celular, Instituto de Investigação e Inovação em Saúde (i3S), Universidade do Porto, 208 Rua Alfredo Allen, 4200-135 Porto, Portugal. ⁴Global Center for Science and Engineering, Faculty of Science and Engineering, Waseda University, 3-4-1 Okubo, Shinjuku-ku, Tokyo 169-8555, Japan. ⁵Institute for Advanced Research of Biosystem Dynamics, Waseda Research Institute for Science and Engineering, Graduate School of Advanced Science and Engineering, Waseda University, 3-4-1 Okubo, Shinjuku-ku, Tokyo 169-8555, Japan. ⁶Komaba Institute for Science, The University of Tokyo, 3-8-1, Komaba, Meguro-ku 153-8902 Tokyo, Japan. ⁷Research Center for Complex Systems Biology, The University of Tokyo, 3-8-1, Komaba, Meguro-ku 153-8902 Tokyo, Japan. ⁸Department of Bioscience, Faculty of Life Science, Okayama University of Science, 1-1 Ridaicho, Kita-ku, Okayama-shi 700-0005, Japan. ⁹Institute for Medical-Oriented Structural Biology, Waseda University, 2-2 Wakamatsucho, Shinjuku-ku, Tokyo 162-8480, Japan. email: masasato@waseda.jp

The dynamic behaviour of microtubules is essential for many aspects of cellular events, including chromosome segregation in dividing cells. Spindle microtubules capture the kinetochore region of chromosomes using the plus end and pull the chromosomes towards the spindle poles (centrosomes or yeast spindle pole bodies (SPBs)) by shortening the microtubules (also called depolymerisation)¹. For chromosome pulling in higher eukaryotes, depolymerisation also occurs at the minus end of spindle microtubules around the poles. In contrast, depolymerisation is observed exclusively at the plus end, which is attached to kinetochores in yeast cells².

By nature, microtubules display a dynamic property called dynamic instability in vitro, facilitating their spontaneous polymerisation and depolymerisation^{3,4}. In cells, this property is further modulated by microtubule-associated proteins (MAPs), allowing microtubules to be transformed according to cellular requirements.

Members of the kinesin-13 subfamily are microtubule depolymerases in higher eukaryotes, working at both ends of microtubules⁵. However, kinesin-13 members are non-existent in the yeast genome, and kinesin-8 drives the depolymerisation of microtubules. Kip3, the budding yeast kinesin-8, depolymerises microtubules in a microtubule length-dependent manner^{6,7}. The kinesin-8 heterodimer Klp5/Klp6 in the fission yeast *Schizosaccharomyces pombe* is involved in microtubule destabilisation rather than depolymerisation^{8–11}. However, chromosome pulling could still be observed in Klp5/Klp6 knockout cells, indicating that other factors, possibly non-motor proteins, might be involved in microtubule shortening in fission yeast^{8,9,12,13}.

Members of the Dis1/TOG family are regulators of microtubule dynamics conserved across species. TOG has been accepted as a processive polymerase for microtubules, which provides tubulin dimers to the plus end^{14–19}. The *S. pombe* genome has two TOG orthologs, Alp14 and Dis1. Both Dis1 and Alp14 in fission yeast contain two tandem TOG domains at their N-termini and have been shown to locate at the plus end to polymerise microtubules^{20–23}. Alp14 was established as the major microtubule polymerase based on in vitro biochemical assays and the phenotype of Alp14 knockout cells. These cells exhibit short and fragile microtubules in the mitotic spindle, as well as in the cytoplasmic and radial arrays during interphase and meiosis^{21–24}.

Dis1, another TOG ortholog, reportedly promotes microtubule elongation in biochemical assays²⁰. However, the phenotype of Dis1 knockouts is puzzling: these cells display cytoplasmic microtubules of normal length similar to wild-type cells, and their dynamics are not largely altered^{25,26}. In mitosis, the spindle in Dis1 knockouts is fragile during prometaphase and considerably extended during anaphase^{11,27}. Furthermore, we have previously reported that chromosome pulling by microtubules was defective in *dis1Δ* meocytes, indicating that Dis1 may depolymerise microtubule plus ends connected to kinetochores²⁴. Dis1 is also involved in shortening guanylyl-($\alpha\beta$)-methylene-diphosphonate (GMPCPP)-stabilised microtubules in vitro²⁰. These findings suggest that Dis1 may play unconventional roles in shortening microtubules for chromosome pulling rather than canonical functions as a microtubule polymerase. Moreover, TOGs in other species may induce microtubule shortening according to circumstances^{28–34}.

Based on the increasing findings, we propose that TOGs may have dual functions in extending or shortening microtubules and that Dis1 could be a previously unidentified candidate involved in microtubule shortening and drives chromosome pulling in concert with kinesin-8. Therefore, we investigated the possibility that Dis1 in fission yeast may shorten microtubules in vitro and in vivo.

Results

Dis1 induces microtubule catastrophe in vitro. In general, Dis1 (aka XMAP215 or TOG) family members are engaged in microtubule polymerisation, as demonstrated in several in vitro and in vivo studies³⁵. Based on the growing evidence of the unique function of Dis1 in microtubule shortening, we examined the effect of Dis1 on microtubules in vitro.

Recombinant GST-Dis1 was incubated with fluorescein-labelled purified porcine tubulin, and microtubule formation was observed under the confocal microscope (Fig. 1a; Supplementary Fig. 1a). Microtubules in the presence of GST-Dis1 tended to shorten (Fig. 1a–c). GST-Dis1 also tended to decrease the number of microtubule bundles. However, this change was not statistically significant (Supplementary Fig. 1b). The decrease of bundles was not accompanied by a reduction in microtubule nucleation, implying that Dis1 does not inhibit nucleation (Supplementary Fig. 1c). The effect of Dis1 on microtubule shortening was further evaluated by the two-step incubation. First, microtubules composed of purified porcine tubulin and fluorescent tubulin (19:1, 38 μ M) were grown at 37 °C for 10 min, and subsequently, GST-Dis1 was added prior to monitoring the microtubule dynamics at 37 °C (Fig. 1d; Supplementary Table 1). Serial images were acquired every 5 s, and average rates for microtubule growth and shrinkage, as well as frequencies of catastrophe (defined as an event in which growth turns into shrinkage) and rescue (an event in which shrinkage turns into growth) were calculated. Microtubule growth was accelerated by GST-Dis1, whereas the shrinkage rate remained constant (Fig. 1e–g; Supplementary Table 1). Notably, GST-Dis1 addition significantly increased the frequency of microtubule catastrophe (Fig. 1e, h; Supplementary Table 1). The frequency of rescue was also increased by GST-Dis1 (Fig. 1i; Supplementary Table 1). As a single catastrophe event quickly shortens microtubules in contrast to slow polymerisation, the net length of each microtubule was shortened in the presence of GST-Dis1 (Fig. 1b, c). Thus, Dis1 promotes microtubule dynamics: it may destabilise microtubules in addition to a known canonical function to grow them.

Dis1 anchored at kinetochores shortens microtubules in meocytes.

As previously demonstrated²⁴, the kinetochores of fission yeast are scattered in the nucleus during the meiotic prophase. They are then collected towards spindle poles at the onset of meiosis I by a radial array of microtubules emanating from the poles. In wild-type (WT) meocytes, Dis1 was located at the plus-end of microtubules as well as kinetochores upon retrieval (Fig. 2a; Supplementary Fig. 2a). In *dis1Δ* (*dis1*-knockout) meocytes, kinetochores were attached by the radial array of microtubules but were frequently uncollected (Fig. 2a). Collectively, these in vitro and in vivo results indicated that Dis1 might induce catastrophe, rather than depolymerisation, thereby shortening microtubules to retrieve kinetochores in WT meocytes. Subsequently, catastrophe frequencies of microtubules in WT meocytes were calculated with regard to the Dis1 location. Microtubules decorated with (ii, Fig. 2b, c; Supplementary Table 2) and without (iii, Fig. 2b, c) Dis1-3GFP at the plus-end tended to undergo catastrophe to a similar degree, although the microtubules with Dis1-3GFP had a slightly higher catastrophe frequency. Notably, catastrophe was significantly promoted when the tip carried kinetochores concomitantly with Dis1 (i), implying that Dis1 and kinetochores synergistically promote catastrophe of the tip ($P < 0.05$, Fig. 2c; Supplementary Table 2). In contrast, the catastrophe frequency of microtubule tips in *dis1Δ* cells remained lower than in that in WT cells, irrespective of possession of kinetochores at the tip (iv, v; Fig. 2b, c; Supplementary Table 2),

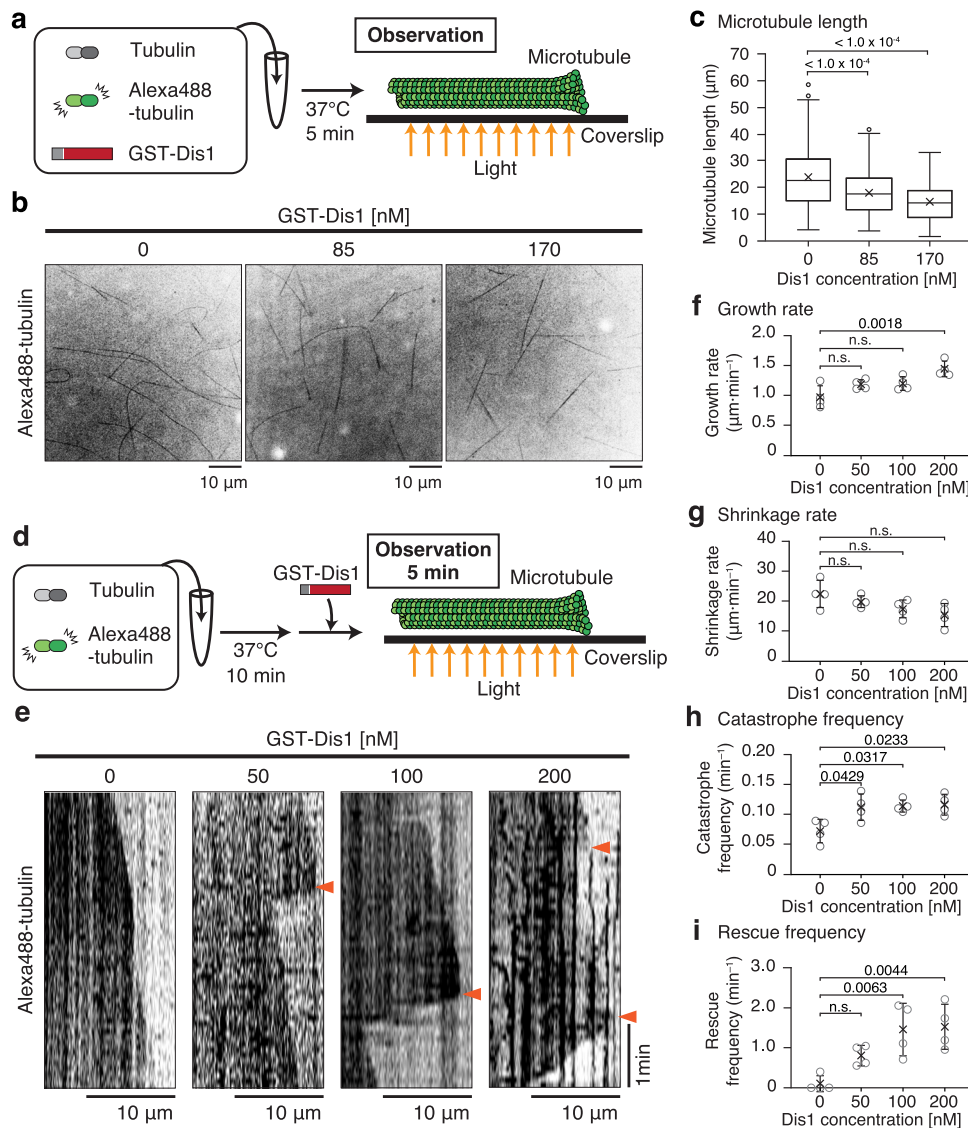


Fig. 1 Dis1 promotes microtubule dynamics in vitro, including induction of catastrophes causing microtubules to shorten. **a** Experimental outline—purified tubulin (20 μM) with Alexa488-labelled tubulins (2 μM) and 0, 85, and 170 nM of recombinant GST-Dis1 were mixed and incubated at 37 $^{\circ}\text{C}$ for 5 min, followed by observation using a confocal microscope. **b** Observed microtubules with and without GST-Dis1. **c** Lengths of microtubules shown in **(b)** were plotted. Box-and-whisker plots indicate the minimum and maximum values and the 25th and 75th percentiles. Bullets indicate outliers; crosses represent means; centre lines represent medians; $n = 156$ (0 nM), 197 (85 nM), 152 (170 nM) microtubules. **d** Experimental outline—purified tubulin (35 μM) with Alexa488-labelled tubulin (3 μM) was incubated at 37 $^{\circ}\text{C}$ for 10 min. GST-Dis1 was then added and observed at 5-s intervals for 5 min using the fluorescent microscope. **e** Representative kymographs for Alexa488-labelled microtubules with indicated concentrations of GST-Dis1. Arrowheads represent the timing of microtubule catastrophes. **f–i** Growth (**f**), shrinkage rates (**g**), catastrophe (**h**), and rescue (**i**) frequencies were calculated. Crosses, the mean; bullets, technical replicates; $n = 4$ (0 nM), 4 (50 nM), 4 (100 nM), 4 (200 nM) experiments. At least 15 microtubules were observed for each experiment. Error bars; SD. The statistical significance of the difference was determined using one-way ANOVA followed by the Tukey–Kramer method. P values are shown; n.s. not significant.

demonstrating that kinetochores do not inherently induce catastrophe in them associating microtubule tips.

To assess whether Dis1 induces catastrophe, particularly when associated with kinetochores, we next employed the *ndc80-21* temperature-sensitive mutant. Ndc80/Hec1 is a component of the outer kinetochore complex^{36–38}, and Dis1 reportedly uses it as a platform to localise to kinetochores²⁷. The *ndc80-21* mutant contains a mutation in an internal loop of Ndc80, which inhibited Dis1–Ndc80 interaction at kinetochores and therefore, Dis1 localisation to the kinetochore–microtubule interface was lost²⁷. The catastrophe frequency was decreased in *ndc80-21* mutant cells, as in *dis1 Δ* cells (Fig. 2d, e; Supplementary Fig. 2b; Supplementary Table 3). The reduction was recovered by an

enforced tethering of Dis1 to Nuf2²⁷ (Fig. 2d, e; Supplementary Fig. 2b; Supplementary Table 3), another component of the Ndc80 complex^{39,40}. Collectively, we conclude that Dis1 actively induces microtubule catastrophe at the tip, particularly when located at kinetochores.

Thus, Dis1 in cells exerts its influence on the catastrophe of microtubule tips in concert with kinetochores. However, the mechanism by which kinetochores trigger the action of Dis1 remains unexplored. To this end, we investigated the behaviour of Dis1 at microtubule tips and observed that Dis1 tended to locate at microtubule tips for extended periods only when accompanied by a kinetochore than in its absence. In 77% of the microtubule shrinkage events we observed, Dis1 was detached from the tip

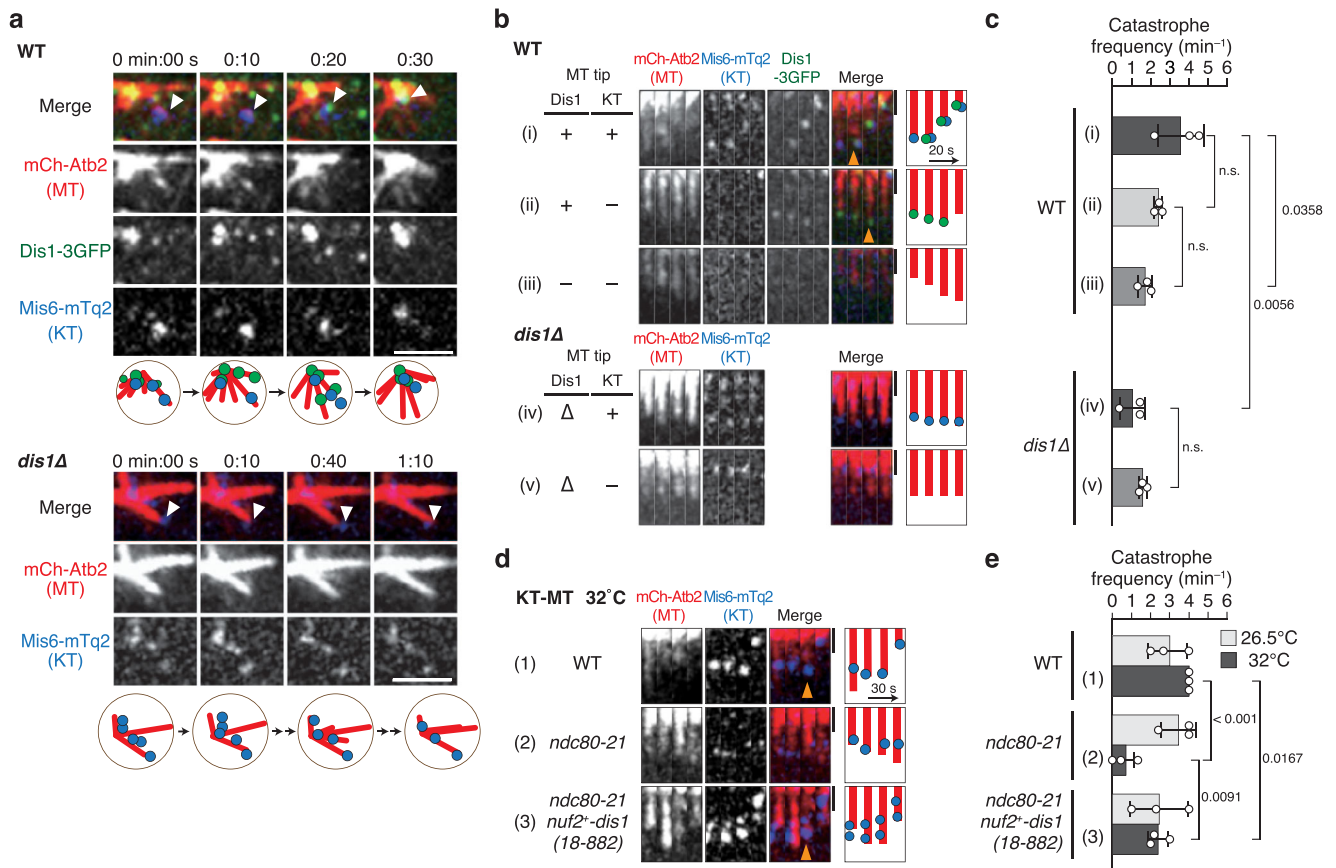


Fig. 2 *Dis1* induces microtubule catastrophe at the onset of meiosis I. **a** Time-lapse images of zygotic nuclei at the onset of meiosis I in wild-type (WT) and *dis1Δ* mutant cells at room temperature. Dis1-3GFP (green) co-localises with kinetochores (KT; labelled with Mis6-mTurquoise2, blue) at microtubule tips (MT; mCherry-Atb2, red). The kinetochore-bound microtubule tip (arrowhead) started shortening at 0:20. Schematics are shown at the bottom. In *dis1Δ*, microtubules attached a kinetochore (arrowhead) but were not shortened. Scale bar, 2 μm. **b** Representative kymographs of microtubules classified by the state of the tips, shown with schematics. In WT, (i) tips with both kinetochores and Dis1; (ii) tips without kinetochores but with Dis1; (iii) tips without kinetochores or Dis1. In *dis1Δ*, with (iv) and without (v) kinetochores. The microtubules in (iv) are also shown in (a). Orange arrowheads represent microtubule catastrophes. Scale bar, 1 μm. **c** The catastrophe frequency for each category in (b); $n = 3$ (i), 3 (ii), 3 (iii), 3 (v) experiments. **d** Representative kymographs for kinetochore-microtubules in (1) WT, (2) *ndc80-21* and (3) *ndc80-21 nuf2⁺-dis1(18-882)* cells at the onset of meiosis I at 32 °C. Orange arrowheads represent microtubule catastrophe. Scale bar, 1 μm. **e** The catastrophe frequency for each state is shown in (d); $n = 3$ experiments for each sample. Bullets indicate technical replicates, and error bars indicate SD. The statistical significance of the difference was determined using one-way ANOVA followed by the Tukey-Kramer method. P values are shown; n.s. not significant.

when it did not accompany kinetochores (i, Fig. 3a; KT: -, Fig. 3b). The frequency of Dis1 that remained at kinetochores during shrinkage was significantly elevated when Dis1 accompanied a kinetochore at the tip (iii, Fig. 3a; 23% [KT: -] and 79% [KT: +] of the events, Fig. 3b). Dis1 tended to accumulate at the tip when attached to the kinetochores during shrinkage, whereas Dis1 unstably fluctuated in the absence of kinetochores (Fig. 3c). Dis1 does not stably locate at the plus tip of microtubules in vivo and in vitro (see Fig. 2b)^{20,26}. Therefore, we propose that kinetochores likely employ the Ndc80 complex²⁷ and serve as a platform to stably retain Dis1 at the shrinking microtubule tip.

Engineered chromosome pulling by Dis1 oligomers placed on a chromosome arm. Our experimental observations led us to postulate that a major function of kinetochores in chromosome pulling is to present Dis1 towards microtubule tips, thereby enabling the stabilisation of kinetochore-microtubule attachment and efficient induction of catastrophe. This hypothesis could be tested by engineering the chromosome arm region from which a cluster of Dis1 may be presented and monitoring whether the Dis1 cluster could attach and shorten the microtubule to retrieve the chromosome arm.

The repetitive sequence of bacterial *lacO* was inserted at the *ade3* locus (approximately 2.4 Mb apart from the centromere of chromosome I) to monitor the site using the associating GFP-fused LacI protein (the *ade3::GFP* strain)^{41,42}. Endogenously expressed Dis1 was fused with the GFP-binding protein (GBP) with or without mCherry^{43,44}. Concordantly, the *ade3::GFP* foci accompanied Dis1-GBP, and were located at non-kinetochore regions, as *ade3::GFP* did not colocalise with the kinetochore marker Mis6-mTurquoise2 (*ade3::GFP* Dis1-GBP-mCherry; Supplementary Fig. 3a). The fluorescence intensity of the Dis1-GBP-mCherry oligomer was comparable to that of Dis1-mCherry (Supplementary Fig. 3b, c). This observation confirmed that Dis1 was artificially installed in the arm region of chromosomes.

The capture of artificial Dis1 oligomers assembled at the *ade3::GFP* locus by the microtubule tip significantly increased the frequency of catastrophe (I, Fig. 4a, b; Supplementary Fig. 3d; Supplementary Table 4) compared to that of free microtubules without *ade3::GFP* foci (II). Although the catastrophe frequency induced by the artificial Dis1 oligomers was moderate compared to that caused by real kinetochores (WT, Fig. 4b; Supplementary Table 4), it was sufficient to retrieve the arm region of chromosome towards SPBs in 71% of cells (Fig. 4c).

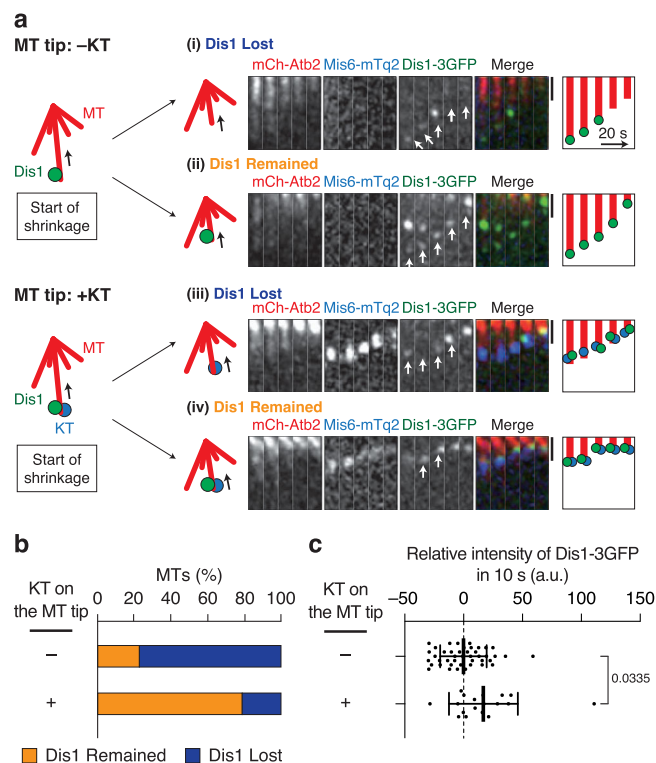


Fig. 3 Kinetochores extend the duration of Dis1 location at the microtubule tip. **a** The fluorescence intensity of Dis1-3GFP localised at the tips of shrinking microtubules was measured in WT cells. Observed microtubules were classified into two groups: tips with Dis1-3GFP only (-KT) and tips with both Dis1-3GFP and kinetochores (+KT). Each group of microtubule tips was then observed over time to monitor the instability of Dis1-3GFP localisation at the tips: whether Dis1-3GFP was lost or decreased ('Dis1 Lost', i and iii), and alternatively, remained or increased ('Dis1 remained', ii and iv) during shrinkage. Representative kymographs and schematics are also shown. White arrows indicate tips of shrinking microtubules where the Dis1-3GFP intensity was measured. The microtubules in which the fluorescence intensities of Dis1-3GFP were lower than the initial value were classified as 'Dis1 Lost', and the rest was classified as microtubules with 'Dis1 Remained'. **b** The rate of each event shown in (a) was quantified. $n = 22$ (-KT), 14 (+KT) microtubules. Dis1 was maintained at the end of microtubules when colocalised with kinetochore according to χ^2 two-sample test ($\chi^2 = 11$, $P < 0.005$). **c** Fluctuation of Dis1-3GFP fluorescence intensity at the tip during shrinkage. The Dis1-3GFP intensity was measured at two time points of a 10-s interval, and the relative intensity of the second time point to the first was plotted. A plot above 0 means an increase of Dis1-3GFP in 10 s. Bold lines means; error bars, SD; $n = 43$ (-KT), 18 (+KT) observations. The statistical significance of the difference was determined using Student's two-tailed t -test; the P value is shown.

In WT meicytes, the kinetochores retrieved up to the SPBs were majorly retained at this position. In contrast, 63% of engineered meicytes detached the *ade3::GFP* foci even after reaching the SPBs (Supplementary Fig. 3e, f). This indicates that the *ade3::GFP* locus presenting Dis1-GBP was unable to maintain the arm region despite being sufficient for retrieval.

To examine whether Dis1 is solely sufficient for chromosome retrieval by microtubules, we monitored the localisation of other kinetochore factors to the artificial *ade3::GFP* site. Representative kinetochore factors such as Mis6 (centromere protein I; CENP-1) of the inner kinetochore complex (constitutive centromere associated network [CCAN]) (Fig. 4a; Supplementary Fig. 3b) as well as Ndc80 (Hec1) of the outer kinetochore network

(KNL-1/Mis12 complex/Ndc80 complex [KMN]) (Supplementary Fig. 4a) were absent from *ade3::GFP* foci. The retrieval of *ade3::GFP* by Dis1-GBP oligomers was also observed in the *nuf2-2* mutant lacking the functional KMN network³⁹, demonstrating that the association of microtubule tips and the *ade3::GFP* locus via Dis1-GBP oligomers were not dependent on other kinetochore factors (Supplementary Fig. 4b–d; Supplementary Table 5). These results demonstrate that oligomerised Dis1 on its own has two potential activities: establishment of stable attachment to microtubule tips and induction of catastrophe.

Retrieval of the *ade3::GFP* site was not associated with the possible recruitment of the microtubule catastrophe factor kinesin-8 (Klp5–Klp6 heterodimer^{8,9,11–13}) because Klp6-3mCherry did not accumulate at the *ade3::GFP* site (Supplementary Fig. 4e). In addition, kinetochores were properly retrieved in *kfp6Δ*, indicating that kinetochore retrieval does not rely on kinesin-8 in meicytes (Supplementary Fig. 4f–h; Supplementary Table 6), although possible recruitment of another unidentified factor that might depolymerise microtubules cannot be completely excluded.

We further focused on the molecular mechanism underlying Dis1-induced catastrophe. In general, TOG domains engage in the regulation of microtubules through binding to tubulin dimers¹⁷. Fission yeast has two paralogous TOG proteins, unlike other eukaryotes. We, therefore, replaced the TOG domains of Dis1 with those of Alp14 and tested its function. When the chimeric protein Alp14^{TOG}-Dis1^C-GBP, comprising N-terminal TOG domains from Alp14 and C-terminal Dis1, was expressed in *ade3::GFP* cells, the chimeric oligomers localised to the *ade3::GFP* foci in a manner similar to that of the original Dis1-GBP oligomers (Supplementary Fig. 3a). The Alp14^{TOG}-Dis1^C-GBP chimera at *ade3::GFP* efficiently contacted microtubule tips; however, they often failed to induce microtubule catastrophe (Fig. 4a, b; Supplementary Fig. 3d; Supplementary Table 4). Dis1-GBP oligomers efficiently induced microtubules to pull the *ade3::GFP* site, whereas the chimeric oligomers failed to perform this function. In contrast, the chimeric oligomers polymerised the microtubule tips (Fig. 4d), probably reflecting the polymerase activity of Alp14 TOGs. The contrast between these two engineered oligomers mimics opposing behaviours of microtubules bound to native kinetochores observed in WT and *dis1Δ* cells (Fig. 4d).

We, therefore, concluded that the TOGs of both Alp14 and Dis1 can promote the attachment of microtubules. Nonetheless, Dis1 is exclusively responsible for the induction of microtubule catastrophe through the action of its TOG domains.

Dis1 induces poleward motion of kinetochores in anaphase A.

Our observations revealed an unconventional function of Dis1, unlike other XMAP215 orthologs, which led us to generalise that Dis1 may also direct chromosome pulling in late mitosis–anaphase A. We monitored the segregation of sister chromatids in mitosis using the *cen2::GFP* system, in which sister centromeres of chromosome II are visualised with GFP⁴¹. Sister chromatids segregated smoothly upon anaphase onset until completion of chromosome pulling, as *cen2::GFP* signals reached SPBs within 1 min (Fig. 5a). In sharp contrast, the completion of pulling took approximately 2–5 min in *dis1Δ* cells (Fig. 5a, Supplementary Fig. 5a). This delay is attributed to an increase in the inter-SPB distance, as well as a frequent pause of microtubules, wherein the dynamics appeared ceased (Fig. 5a, b, Supplementary Fig. 5b, c). These events could be interpreted as microtubule stabilisation caused by the reduction of catastrophe. Concordantly, the frequency of catastrophe that induces the transition from pause to depolymerisation was decreased in *dis1Δ* cells (Fig. 5c).

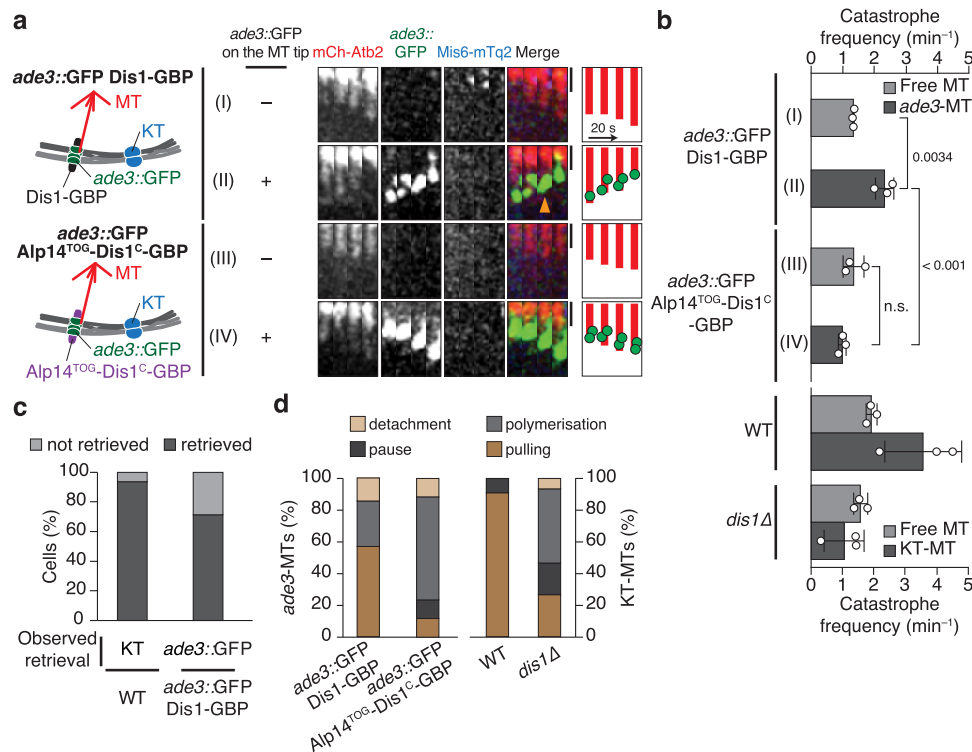


Fig. 4 End-on pulling of chromosomes by Dis1 oligomers without using kinetochores. **a** Schematic representation of the artificial pulling of chromosomes without relying on kinetochores. Oligomers of Dis1-GBP or the chimaera Alp14^{TOG}-Dis1^C-GBP were artificially clustered at the *ade3* locus marked with GFP (*ade3::GFP*, green) on a chromosome arm. Time-lapse images of microtubules without (I and III) or with (II and IV) the *ade3::GFP* locus were filmed at room temperature, and representative kymographs are shown. As a reference, the position of kinetochores (Mis6-mTq2, blue) is shown. The orange arrowhead indicates the start of the microtubule catastrophe. Scale bar, 1 μ m. **b** The catastrophe frequency was measured for each category in (a). Free MT, tips without kinetochores; *ade3*-MT, tips with *ade3::GFP*. The data for WT and Dis1 are reprised from previous data as references: the data for 'free MT' in WT are derived from Fig. 2c (ii and iii). Other data for WT and *dis1 Δ are reprises of Fig. 2c (i, iv and v). Bullets indicate technical replicates ($n = 3$ experiments); error bars, SD. The statistical significance of the difference was determined using one-way ANOVA followed by the Tukey-Kramer method. P values are shown; n.s., not significant. **c** Percentages of cells that accomplished retrieval of chromosomes to SPBs in WT meicyotes (WT, $n = 16$) or retrieval of the *ade3::GFP* locus in *ade3::GFP* Dis1-GBP meicyotes ($n = 28$). $\chi^2 = 3.1$ (two-sample test), $P > 0.05$. **d** Frequencies of 4 events (polymerisation, pulling, pause and detachment) observed in microtubule tips accompanied by the *ade3::GFP* locus or kinetochores. $n = 11$ (WT), 15 (*dis1 Δ), 14 (*ade3::GFP* Dis1-GBP), 17 (*ade3::GFP* Alp14^{TOG}-Dis1^C-GBP) microtubules.**

Frequent pausing was similarly observed in the *alp14*^{TOG}-*dis1*^C mutant, in which the TOG domain of Dis1 was replaced by that of the Alp14 chimeric protein (Fig. 5a–c). Although the chimeric mutant exhibited moderate defects in catastrophe induction (Fig. 5c), the double mutant of *alp14*^{TOG}-*dis1*^C *klp6 Δ was lethal (see Discussion, Supplementary Fig. 5d), suggesting that TOGs in Alp14 do not possess any adequate activities for catastrophe induction. These results collectively demonstrate that TOG domains of Dis1 are required for the induction of catastrophe and are incompatible with those of Alp14.*

Discussion

Promoting catastrophe is essential in fission yeast meicyotes for the conversion of kinetochore positioning at the entry into meiosis I²⁴. Kinetochore pulling is primarily operated by the non-motor/non-kinesin protein Dis1 as a knockout of kinesin-8 (Klp5/6 heterodimers), which has been regarded as microtubule destabilizer in this organism^{8,9,11–13}, caused no apparent defects in kinetochore pulling in meicyotes. At least in meiosis, kinetochore pulling force may be mainly generated by Dis1 and supportively by kinesin-8. This study revealed the unconventional activity of Dis1 to induce microtubule catastrophe in vitro, although TOG family members have been generally characterised or regarded as microtubule polymerase^{14,15,17–23,35}. When catastrophe is induced, Dis1 may not catalyse GTP-bound tubulin

into GDP, because it has been shown that Dis1, in the absence of free tubulin, is shown to depolymerise GMPCPP-microtubules that cannot be hydrolysed²⁰. Dis1 also induces catastrophe in mitotic cells (anaphase A) in addition to kinesin-8 (Klp5–Klp6), as supported by the fact that double knockout of *klp5* (or *klp6*) and *dis1* is synthetically lethal¹³. The TOG domains of Dis1 are responsible for catastrophe induction during chromosome pulling in meiosis and mitosis, which are incompatible with the TOGs of Alp14.

The mechanisms underlying the functional difference of Alp14 and Dis1, two TOG/XMAP215 paralogs in *S. pombe*, remain unknown. Recently, X-ray crystallography-based studies revealed that two TOG domains of Alp14 were spatially aligned in tandem, which may be crucial for Alp14 as a polymerase to attach a tubulin dimer that is eventually deposited to a microtubule tip⁴⁵. The AlphaFold algorithm^{46,47} (<https://alphafold.ebi.ac.uk/>) was recently used to predict the similar tandem alignment of two TOGs in Alp14, whereas those in Dis1 were predicted in an antiparallel alignment with a certain degree of flexibility (schematics are shown in Fig. 6a). The flexibility of Dis1 TOGs in the structure might enable the dissociation, rather than association, of tubulin dimers from the microtubule tips, thereby possibly inducing catastrophe.

XMAP215/TOG proteins reportedly possess the activity of the microtubule polymerase; however, XMAP215 orthologs occasionally

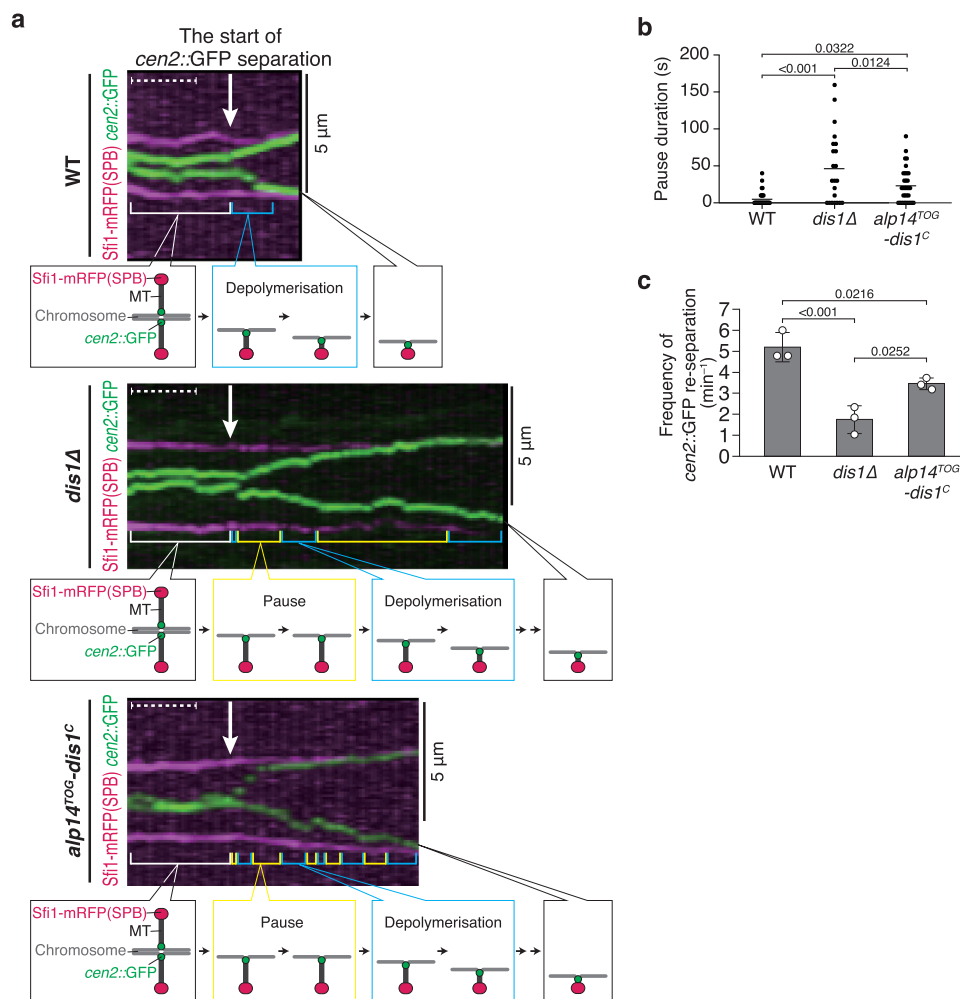


Fig. 5 Dis1 drives kinetochore motion during Anaphase A in mitosis. **a** Representative kymographs depicting the distribution of sister centromeres of chromosome II labelled with GFP (*cen2::GFP*, green) in WT, *dis1Δ* and *alp14^{TOG}-dis1^C* cells during anaphase A of mitosis at room temperature. Spindle poles (SPBs) were visualised with Sfi1-mRFP (magenta). Arrows represent the timing when *cen2::GFP* signals started to separate. Blue brackets denote the shortening of the distance between an SPB and *cen2::GFP*, and yellow brackets denote the pause of the *cen2::GFP* signal. Dashed lines correspond to 1 min. **b** Pause duration of *cen2::GFP* in Anaphase A of each strain was plotted. $n = 33$ (WT), 22 (*dis1Δ*), 32 (*alp14^{TOG}-dis1^C*) centromeres. Lines represent means. **c** The frequency of *cen2::GFP* re-separation after a pause was calculated. Bullets indicate technical replicates ($n = 3$ experiments); error bars, SD. The statistical significance of the difference was determined using one-way ANOVA followed by the Tukey-Kramer method. P values are shown; n.s. not significant.

destabilise microtubules. *Xenopus* XMAP215 depolymerises GMPCPP microtubules in the egg extract²⁸ and increases both the growth and shrinkage rates of microtubules²⁹. The stabilisation activity in the egg extract appears to be induced through phosphorylation³⁰. In vitro studies also reported the activity of *Xenopus* XMAP215 and *tobacco* MAP200 in the induction of catastrophe: this could be due to indirect effects by a simultaneous increase of the microtubule growth rate, which consequently caused an uneven extension of some protofilaments and triggered catastrophe^{48,49}. In contrast, fission yeast Dis1 appears to directly induce catastrophe during meiosis and mitosis, as microtubule growth was not enhanced during Dis1 localisation at the microtubule tips (see Figs. 2a and 4d).

In the mutants of budding yeast Stu2, the microtubule dynamics are reduced in interphase and mitosis during chromosomal attachment^{31,32}. Stu2 increased the catastrophe frequency of porcine microtubules³³ but decreased that of yeast microtubules⁵⁰ in vitro. Stu2 at kinetochores stabilises kinetochore-microtubule attachment⁵¹, whereas it also may indirectly contribute to the movement of kinetochores coupled

with microtubule depolymerisation in a ‘catch-bond’ manner³⁴. Although still controversial, Stu2 may possess activities for both polymerase and catastrophe factors. Our study clarifies the major function of Dis1 in vivo as a direct catastrophe inducer, which is sufficient for poleward chromosome movement.

Our live-cell imaging for meicytes demonstrated that Dis1 is mainly delivered to kinetochores via tips of growing microtubules (see Fig. 2a, Supplementary Fig. 3a), although Dis1 may stochastically be detached from the tips (i; Fig. 6b). The other TOG ortholog Alp14 is responsible for the growth of the microtubules²⁴. Once a microtubule tip reaches a kinetochore, Alp14 stabilises its attachment^{52,53}. Concomitantly, Dis1 is locked to the microtubule-kinetochore interface by the outer kinetochore factor Ndc80 (Fig. 3)²⁷, which enables repetitive catastrophe to shorten microtubules carrying kinetochores until they reach spindle poles (ii, iii; Fig. 6b).

This may be related to a possible discrepancy in the preceding experiments by Matsuo et al.²⁰, in which induction of catastrophe by Dis1 was not evident. In our in vitro assays, a higher concentration (50–200 nM) of recombinant Dis1 proteins was used

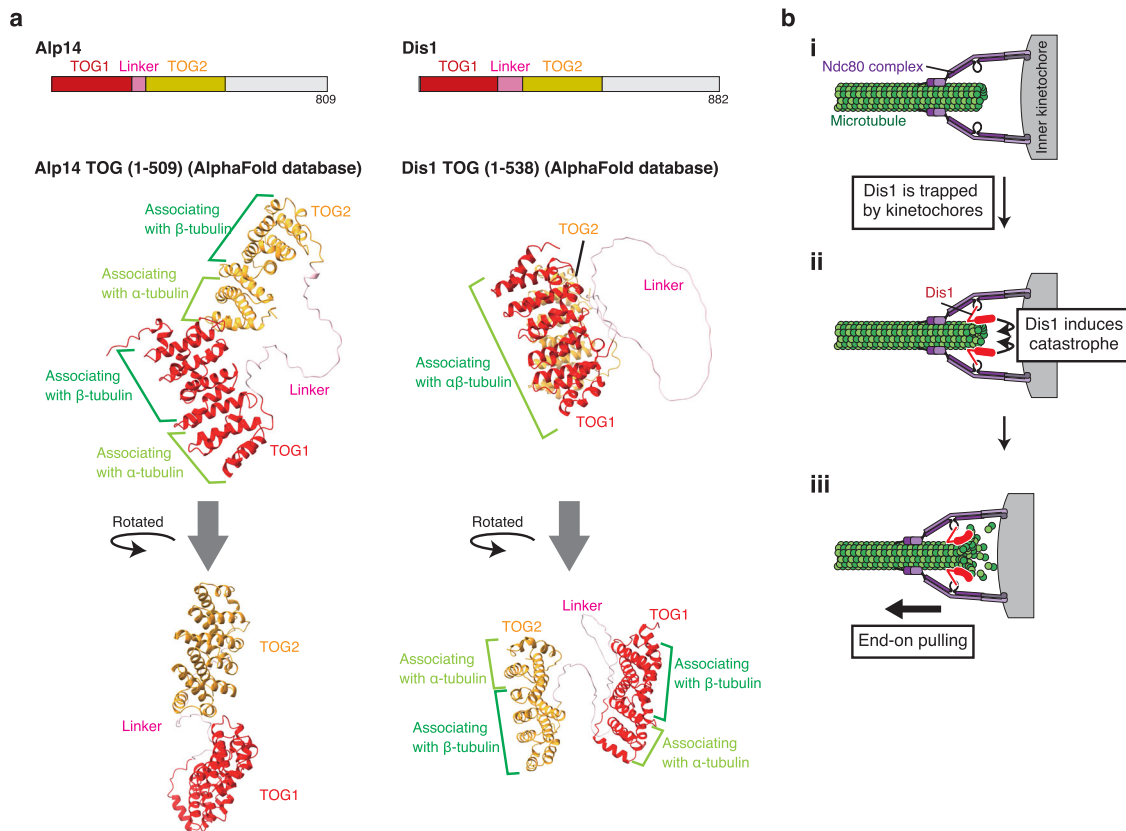


Fig. 6 Comparison of the predicted structures of TOG domains between Alp14 and Dis1. **a** Predicted structures of the TOG domain of Alp14 (1-509 a.a.) and that of Dis1 (1-538 a.a.) were referred to the AlphaFold database (<https://alphafold.ebi.ac.uk/>)⁴⁷. Domains for TOG1, linker and TOG2 are shown in red, pink and yellow, respectively, using ChimeraX v.1.2.5. (UCSF)⁶⁹. The style of association between tubulin dimers and each TOG was adapted from a previous study on Alp14 crystallography⁴⁵. **b** Possible schemes representing kinetochore retrieval by Dis1. First, the kinetochore attaches to the microtubule, which does not actively promote catastrophe (i). Upon reaching the microtubule tip, Dis1 is trapped by kinetochores and induces catastrophe (ii), which triggers microtubule shrinkage, thereby retrieving the kinetochore (iii).

when frequent microtubule catastrophe was demonstrated. Such a high concentration of Dis1 *in vitro* might simulate intense accumulation of Dis1 *in vivo*, locked at microtubule tips by kinetochore factors. Artificial Dis1 oligomers are sufficient to induce microtubule catastrophe and to pull chromosome arms. Therefore, we conclude that the whole kinetochore organisation is not required for microtubule-mediated chromosomal pulling. In contrast, the role of the kinetochore is to tightly lock Dis1 to the kinetochore-microtubule interface using the Ndc80 complex²⁷.

Dis1 is critical for both attachments to microtubule tips and the generation of chromosome-pulling force. Therefore kinetochore pulling at meiosis I onset was emulated by Dis1 oligomers on a chromosome arm. More complex systems, however, would be required when we emulate the entire scenarios for chromosome segregation. For instance, kinetochore pulling at meiosis I onset is monopolar attachment, whereas chromosome segregation is bipolar. This requires additional systems to mimic the ‘search and capture’ behaviour to establish bipolar attachment. Additional factors such as Mal3 (EB1) would be required, as Mal3 may also contribute to the establishment of the attachment through interaction with Dis1²⁰. These may be further assessed by reconstruction of kinetochore-microtubule attachment *in vitro*, using recombinant proteins as well as tubulin purified from the porcine brain or *S. pombe* cells.

In addition, our experiments also demonstrated that retrieved chromosomes by artificial Dis1 oligomers could not be maintained at spindle poles. The retention may require the long-term lateral connection of microtubules and chromosomes. Dis1 might

not generate the sufficient force on the lateral surface of microtubules²⁰, and the outer kinetochore components represented by Ndc80 would be required for efficient retention^{36,54}. Identifying such factors would contribute to the generation of an artificial system for chromosome segregation in the future.

Methods

Data reporting. No statistical methods were used to predetermine the sample size. The experiments were not randomised. The investigators were not blinded to allocation during experiments and outcome assessment. All source data underlying the graphs presented in the main and supplementary figures were uploaded as Supplementary Data online.

Yeast strains, media and genetics. Standard materials and methods were used for *S. pombe* biology⁵⁵. Yeast strains used in this study are listed in Supplementary Table 7. For vegetative growth of *S. pombe* cells, YE5S (yeast extract with supplements) was used. To induce mating and meiosis, homothallic (*h*⁹⁰) cells grown in YE5S were spotted on sporulation agar (SPA) plates.

Standard materials and methods were used for knock-in and knock-out of genes unless otherwise specified^{56–58}. For the visualisation of microtubules, coding sequences for mCherry and Atb2 (α -tubulin) were fused in the frame and flanked with the native promoter and terminator for the *atb2*⁺ gene. The gene construct was then integrated into the Z2 region on chromosome II as an extra copy of the endogenous *atb2*⁺ gene, and the resultant strain is referred to as ‘Z2-mCherry-atb2’ in the list (Supplementary Table 7)⁵⁹. For tagging of the mTurquoise2 fluorescent protein to Mis6, a pFA6a-based plasmid containing the mTurquoise2 sequence and the natMX6 selection marker was created (named as pMS-mTurquoise2-nat, NBRP ID: FYP5207) and used for polymerase chain reaction (PCR)-based gene tagging as usual.

For visualisation of the position of the *ade3*⁺ locus on chromosome I, the canonical system utilising the bacterial lactose operator–repressor (*lacO*–*LacI*) was introduced^{41,42,60–62}. The *h*⁹⁰ strain that contains the repetitive *lacO* sequences at the *ade3*⁺ locus (*ade3::lacO*) and expresses the fusion protein *LacI*-NLS-GFP

(the *ade3::GFP* strain hereafter) was originally gifted by A. Yamamoto, Y. Hiraoka and M. Yamamoto.

The *ade3::GFP* strain was then genetically crossed with strains harbouring the Dis1-GBP or Dis1-GBP-mCherry fusion gene constructs⁴⁴. The resultant strains are expected to display Dis1-GBP or Dis1-GBP-mCherry oligomers at the *ade3* locus, respectively, in concert with LacI-NLS-GFP clustered at the *ade3::lacO* locus.

The *ndc80-21* strains with or without the *nuf2⁺-dis1(18-882)* fusion gene was gifted by T. Toda²⁷. The *nuf2-2* strain was originally gifted by Y. Hiraoka³⁹.

The strain in which the TOG domains of Dis1 were replaced with those of Alp14 (Alp14^{TOG}-Dis1^C) was constructed as follows: first, the chimeric gene construct containing the N-terminal region of Alp14 (1–500 residues) fused with the C-terminus of Dis1 (518–882), flanked by 5′- and 3′-UTR regions of the *dis1⁺* gene, was prepared via PCR. The product was then introduced into *dis1::ura4⁺* cells for counter-selection of *ura4⁺* strains using YE5S plates containing 1 mg ml⁻¹ 5-fluoroorotic acid (FOA). The resultant strain *dis1::alp14^{TOG}-dis1^C*, therefore, expresses the fusion protein Alp14^{TOG}-Dis1^C at the endogenous level instead of Dis1. The *bsd* marker gene conferring blasticidin S resistance was inserted downstream of the regions of *dis1⁺* gene to construct the *alp14^{TOG}-dis1^C-bsd* strain.

Centromeres on chromosome II were visualised using the previous system utilising the *cen2::GFP* system, which consists of the *cen2::lacO* insertion with LacI-NLS-GFP in the *h⁹⁰* strain. The original *cen2::GFP* strain used herein was gifted by A. Yamamoto and Y. Hiraoka⁴¹.

Protein expression and purification. Standard methods for recombinant protein expression in bacterial cells were used, as previously summarised⁶³. To express recombinant GST-Dis1 and GST proteins in *E. coli* BL21 (DE3) cells, the coding sequence for *dis1⁺* was cloned into pGEX-KG using *SacI* and *XbaI* sites (pGEX-KG-dis1, NBRP ID: FYP5208). *E. coli* cells containing plasmids were cultured in 2xYT medium at 36 °C overnight. After dilution, cells were further grown for 2 h until OD₆₀₀ reaches 0.2–0.4. IPTG was then added (final 0.2 mM) for 3 h at 30 °C or for 12–24 h at 20 °C to induce expression. Cells were harvested by centrifugation at 5000 rpm for 5 min, 4 °C, and washed twice with PBS and PBS* (PBS with detergents and protease inhibitors). Cells were suspended with PBS* and lysed by sonication of repetitive ‘1-s pulse and 1-s interval’ for 1 min using the sonicator VP-50 (TAITEC). Cell debris was removed by centrifugation (5,000 rpm for 1 min at 4 °C, followed by additional rounds of 14,000 rpm 1 or 3 min 4 °C, ≥2 times), and the supernatant was collected. Glutathione Sepharose 4B (GE Healthcare Life Sciences) was added and mixed for an hour at 4 °C. The Sepharose beads were then poured into a column and washed with PBS* for 3 times. Sepharose-bound GST and GST-Dis1 proteins were eluted with the elution buffer (10 mM L-Glutathione, 50 mM Tris-HCl, pH 8.0). Eluted samples were successively fractionated into tubes. Purified protein samples were once frozen in liquid N₂ and then stored at –80 °C. Sample preparation was confirmed through SDS-PAGE followed by Biosafe-Coomassie (BIO-RAD) staining.

Non-labelled tubulin was purified from porcine brains by four cycles of temperature-regulated polymerisation and depolymerisation in a high molarity PIPES buffer to remove contaminating MAPs⁶⁴. The purified tubulin was flash-frozen and stored in liquid nitrogen.

Turbidity assay. Turbidity assay was performed as previously described¹⁸. Recombinant GST-Dis1 and GST were mixed on ice with 26 μM tubulin in BRB80 buffer (80 mM PIPES, 1 mM MgCl₂, 1 mM EGTA, pH 6.8) containing 1 mM GTP. Microtubule polymerisation was induced by a temperature shift to 37 °C, and the absorbance was monitored at 350 nm in 5-s intervals for 40 min using the spectrometer UV1800 (SHIMADZU) equipped with TCC-240A (SHIMADZU).

Microscopy for in vitro assays. Microscopy regarding in vitro assays for tubulin dynamics was performed as previously described⁶⁵ with the following minor modification. Briefly, we used the inverted microscope ECLIPSE Ti (Nikon) equipped with the scanner unit CSU-W1 (Yokogawa) and the sCMOS camera Zyla 4.2 operated by the software IQ3 (Andor). To control the stage temperature, a stage-top incubator system composed of a customised double ThermoPlate chamber (11.5 × 7.5 × 0.3 cm inside size) and a TP-LH lens heater (TOKAI HIT) were used.

For visualisation of microtubules, Alexa488 (Alexa Fluor 488 NHS Ester, Thermo Fisher Scientific) labelled tubulin, and unlabelled tubulin was mixed at a volume ratio of 1:19. To measure the number and length of microtubule in the presence of recombinant proteins (GST-Dis1 or GST), 22 μM pre-mixed tubulin and the recombinant proteins were mixed in BRB80 containing 0.57 mM GTP on ice. The solution was applied on a glass slide and enclosed with a cover slip (Matsunami glass) immersed with ethanol and then dry them before use. Microtubule polymerisation was induced at 37 °C for 5 min and then started observation. Fiji was used for quantification⁶⁶. Microtubules extending out of the image were not included.

The dynamics of microtubules were analysed as follows. First, 38 μM pre-mixed tubulin in BRB80 containing 1 mM GTP was incubated for 10 min at 37 °C. The solution was then mixed with an equal volume of a pre-warmed mixture comprising the observation buffer [0.8% Catalase (Sigma), 200 (U ml⁻¹) Glucose oxidase (Sigma), 9 mg ml⁻¹ Glucose, 2 mM MgCl₂, 2 mM GTP, 1% (v v⁻¹) 2-mercaptoethanol] and recombinant proteins (GST-Dis1 or GST). Coverslips were

immersed in ethanol and then dry them before use. Serial images were acquired every 5 s. Acquired images were converted from 16-bit to 8-bit, and kymographs were generated using Fiji. In Fig. 1, images were shown in black/white inversion.

Microscopy for cells. Our standard methods were applied as previously described⁵⁸. Briefly, the observation system comprised the DeltaVision-SoftWoRx image acquisition system (Applied Precision) equipped with Olympus inverted microscopes IX71 and IX81 and CoolSNAP HQ2 CCD cameras (Photometrics).

For the live-cell imaging of meiotic cells, homothallic (*h⁹⁰*) cells were spotted onto SPA and incubated for 12–13 h at 26.5 °C for induction of meiosis, and an additional 2 h at 32 or 36 °C if necessary for temperature-sensitive strains. Cells were then mounted on a glass-bottom dish (Iwaki glass or Matsunami glass) precoated with lectin from Glycine max (Sigma). Prior to observation, the dish was filled with EMM–N + C + U + L, minimal media without a nitrogen source supplemented with uracil (50 μg ml⁻¹) and leucine (100 μg ml⁻¹) prewarmed according to the observation temperature. Images of 5–10 sections along the z-axis were acquired at 0.4-μm intervals.

For the filming of mitotic cells, cells were cultivated at 30 °C overnight prior to observation in the SD medium supplemented with alanine (75 μg ml⁻¹), uracil (50 μg ml⁻¹), lysine (50 μg ml⁻¹), leucine (100 μg ml⁻¹), and histidine (50 μg ml⁻¹). Cells were mounted on a glass-bottom dish as mentioned above, and the dish was filled with EMM + N + C + 5 S, minimal media with a nitrogen source supplemented with alanine, uracil, lysine, leucine, and histidine.

Images taken along the z-axis were deconvoluted and projected into a single image using the SoftWoRx software (v3.7.0 and v.6.5.1), and the resolution was adjusted using Adobe Photoshop CC (version 2022).

The fluorescence intensity of GFP- or mCherry-tagged Dis1 in cells was quantified using SoftWoRx as follows: acquired images were projected into a single image using the Sum projection algorithm without deconvolution. A punctate signal of Dis1-GFP or Dis1-GBP-mCherry in 3 × 3 pixels was quantified using SoftWoRx, and the background signal taken outside of the nucleus was subtracted.

Image analyses. To measure the parameters of microtubule dynamics in vitro, image stacks were analysed using Fiji. Then the position of the microtubule end was tracked using the MTrack J plugin for Fiji⁶⁷. The distance between both ends was calculated, and the transition events from microtubule growth to shrinkage were defined as catastrophe, and events from shrinkage to growth as a rescue. Four parameters describing the microtubule dynamics were calculated. Growth and shrinkage rates were calculated as average values. Frequencies of catastrophe and rescue were calculated as follows: the total number of catastrophe events was divided by the total time for microtubule growth. Kymographs were created by use of Fiji.

To measure microtubule dynamics in cells at the onset of meiosis, kymographs were created as follows: the microtubule region of interest was cropped into strips and aligned in the course of time using Adobe Illustrator CC (version 2022). The catastrophe frequency was then calculated as described above. Each section along the z-axis was analysed to confirm that the microtubule end (GFP-Atb2), Dis1-3GFP and kinetochores (marked by Mis6-mTurquoise2) are co-localised on a single plane.

The SoftWoRx software was used for tracking *cen2::GFP* punctate signals in mitotic cells and the creation of kymographs. To measure the dynamic behaviour of *cen2::GFP* dots in relation to Sfi1-mCherry (an SPB marker), sequential images were applied to Fiji. The distance between a Sfi1-mCherry dot (SPB) and *cen2::GFP* (centromere) was chased over time to calculate the microtubule dynamics: pause and depolymerisation. ‘Pause’ was defined as duration without detectable motion of a *cen2::GFP* dot, whereas ‘depolymerisation’ as duration with the poleward movement of *cen2::GFP* that corresponds to sister chromatid separation in anaphase A. When a paused *cen2::GFP* started to move poleward again, this depolymerisation event was particularly defined as ‘re-separation’ of *cen2::GFP*.

Statistics and reproducibility. The methods used to test for differences in statistically significant are described in each figure legend. The R package multcomp ver.1.4-19⁶⁸ were used to measure the statistical significance of difference by one-way ANOVA followed by the Tukey–Kramer method. Microsoft Excel software was used to perform Student’s two-tailed *t*-test and χ^2 two-sample test. *P* values are shown on top of the corresponding columns. If the *P*-value was >0.05, it was stated as not significant. When representative images are shown, at least three repeats were performed except for Supplementary Figs. 1a, 2a, 3a, b, 4a, e and 5d. Two repeats were performed for Supplementary Figs. 2a, 3a, b, 4a, e and 5d. The repeats are not necessary for Supplementary Fig. 1a because it represents purified proteins used in Fig. 1.

Reporting summary. Further information on research design is available in the Nature Portfolio Reporting Summary linked to this article.

Data availability

The data presented in this study are available from the corresponding author upon reasonable request. Plasmids constructed in this study have been deposited with NBRP

(National BioResource Project), Japan: pMS-mTurquoise2-nat (NBRP ID: FYP5207) and pGEX-KG-dis1 (NBRP ID: FYP5208). The source data of the graphs are provided as a Supplementary Data file.

Received: 5 August 2022; Accepted: 16 November 2022;

Published online: 26 November 2022

References

- Walczak, C. E. & Heald, R. Mechanisms of mitotic spindle assembly and function. *Int. Rev. Cytol.* **265**, 111–158 (2008).
- Asbury, C. L. Anaphase a: disassembling microtubules move chromosomes toward spindle poles. *Biology* **6**, 15 (2017).
- Mitchison, T. & Kirschner, M. Dynamic instability of microtubule growth. *Nature* **312**, 237–242 (1984).
- Horio, T. & Hotani, H. Visualization of the dynamic instability of individual microtubules by dark-field microscopy. *Nature* **321**, 605–607 (1986).
- Desai, A., Verma, S., Mitchison, T. J. & Walczak, C. E. Kin I kinesins are microtubule-destabilizing enzymes. *Cell* **96**, 69–78 (1999).
- Gupta, M. L., Carvalho, P., Roof, D. M. & Pellman, D. Plus end-specific depolymerase activity of Kip3, a kinesin-8 protein, explains its role in positioning the yeast mitotic spindle. *Nat. Cell Biol.* **8**, 913–923 (2006).
- Varga, V., Leduc, C., Bormuth, V., Diez, S. & Howard, J. Kinesin-8 motors act cooperatively to mediate length-dependent microtubule depolymerization. *Cell* **138**, 1174–1183 (2009).
- West, R. R., Malmstrom, T., Troxell, C. L. & McIntosh, J. R. Two related kinesins, *kfp5⁺* and *kfp6⁺*, foster microtubule disassembly and are required for meiosis in fission yeast. *Mol. Biol. Cell* **12**, 3919–3932 (2001).
- Garcia, M. A., Koonrugsa, N. & Toda, T. Two kinesin-like kin I family proteins in fission yeast regulate the establishment of metaphase and the onset of anaphase A. *Curr. Biol.* **12**, 610–621 (2002).
- Tischer, C., Brunner, D. & Dogterom, M. Force- and kinesin-8-dependent effects in the spatial regulation of fission yeast microtubule dynamics. *Mol. Syst. Biol.* **5**, 250–250 (2009).
- Pinder, C., Matsuo, Y., Maurer, S. P. & Toda, T. Kinesin-8 and Dis1/TOG collaborate to limit spindle elongation from prophase to anaphase A for proper chromosome segregation in fission yeast. *J. Cell Sci.* **132**, jcs232306 (2019).
- West, R. R., Malmstrom, T. & McIntosh, J. R. Kinesins *kfp5⁺* and *kfp6⁺* are required for normal chromosome movement in mitosis. *J. Cell Sci.* **115**, 931–940 (2002).
- Garcia, M. A., Koonrugsa, N. & Toda, T. Spindle-kinetochore attachment requires the combined action of Kin I-like *Klp5/6* and *Alp14/Dis1*-MAPs in fission yeast. *EMBO J.* **21**, 6015–6024 (2002).
- Gard, D. L. & Kirschner, M. W. A microtubule-associated protein from *Xenopus* eggs that specifically promotes assembly at the plus-end. *J. Cell Biol.* **105**, 2203–2215 (1987).
- Brouhard, G. J. et al. XMAP215 is a processive microtubule polymerase. *Cell* **132**, 79–88 (2008).
- Severin, F., Habermann, B., Huffaker, T. & Hyman, T. Stu2 promotes mitotic spindle elongation in anaphase. *J. Cell Biol.* **153**, 435–442 (2001).
- Al-Bassam, J., Breugel, M., van, Harrison, S. C. & Hyman, A. Stu2p binds tubulin and undergoes an open-to-closed conformational change. *J. Cell Biol.* **172**, 1009–1022 (2006).
- Hamada, T., Igarashi, H., Itoh, T. J., Shimmen, T. & Sonobe, S. Characterization of a 200 kDa microtubule-associated protein of tobacco BY-2 cells, a member of the XMAP215/MOR1 family. *Plant Cell Physiol.* **45**, 1233–1242 (2004).
- Charrasse, S. et al. The TOGp protein is a new human microtubule-associated protein homologous to the *Xenopus* XMAP215. *J. Cell Sci.* **111**, 1371–1383 (1998).
- Matsuo, Y. et al. An unconventional interaction between Dis1/TOG and Mal3/EB1 in fission yeast promotes the fidelity of chromosome segregation. *J. Cell Sci.* **129**, 4592–4606 (2016).
- Garcia, M. A., Vardy, L., Koonrugsa, N. & Toda, T. Fission yeast ch-TOG/XMAP215 homologue *Alp14* connects mitotic spindles with the kinetochore and is a component of the Mad2-dependent spindle checkpoint. *EMBO J.* **20**, 3389–3401 (2001).
- Nakaseko, Y., Goshima, G., Morishita, J. & Yanagida, M. M phase-specific kinetochore proteins in fission yeast: microtubule-associating Dis1 and Mtc1 display rapid separation and segregation during anaphase. *Curr. Biol.* **11**, 537–549 (2001).
- Al-Bassam, J. et al. Fission yeast *Alp14* is a dose-dependent plus end-tracking microtubule polymerase. *Mol. Biol. Cell* **23**, 2878–2890 (2012).
- Kakui, Y., Sato, M., Okada, N., Toda, T. & Yamamoto, M. Microtubules and Alp7–Alp14 (TACC-TOG) reposition chromosomes before meiotic segregation. *Nat. Cell Biol.* **15**, 786–796 (2013).
- Nabeshima, K. et al. p93dis1, which is required for sister chromatid separation, is a novel microtubule and spindle pole body-associating protein phosphorylated at the Cdc2 target sites. *Genes Dev.* **9**, 1572–1585 (1995).
- Roque, H., Ward, J. J., Murrells, L., Brunner, D. & Antony, C. The fission yeast XMAP215 homolog Dis1p is involved in microtubule bundle organization. *PLoS ONE* **5**, e14201 (2010).
- Hsu, K.-S. & Toda, T. Ndc80 internal loop interacts with Dis1/TOG to ensure proper kinetochore-spindle attachment in fission yeast. *Curr. Biol.* **21**, 214–220 (2011).
- Shirasu-Hiza, M., Coughlin, P. & Mitchison, T. Identification of XMAP215 as a microtubule-destabilizing factor in *Xenopus* egg extract by biochemical purification. *J. Cell Biol.* **161**, 349–358 (2003).
- Vasquez, R. J., Gard, D. L. & Cassimeris, L. XMAP from *Xenopus* eggs promotes rapid plus end assembly of microtubules and rapid microtubule polymer turnover. *J. Cell Biol.* **127**, 985–993 (1994).
- Vasquez, R. J., Gard, D. L. & Cassimeris, L. Phosphorylation by CDK1 regulates XMAP215 function in vitro. *Cell Motil. Cytoskel.* **43**, 310–321 (1999).
- Kosco, K. A. et al. Control of microtubule dynamics by Stu2p is essential for spindle orientation and metaphase chromosome alignment in yeast. *Mol. Biol. Cell* **12**, 2870–2880 (2001).
- He, X., Rines, D. R., Espelin, C. W. & Sorger, P. K. Molecular analysis of kinetochore-microtubule attachment in budding yeast. *Cell* **106**, 195–206 (2001).
- Breugel, M., van, Drechsel, D. & Hyman, A. Stu2p, the budding yeast member of the conserved Dis1/XMAP215 family of microtubule-associated proteins is a plus end-binding microtubule destabilizer. *J. Cell Biol.* **161**, 359–369 (2003).
- Humphrey, L., Felzer-Kim, I. & Joglekar, A. P. Stu2 acts as a microtubule destabilizer in metaphase budding yeast spindles. *Mol. Biol. Cell* **29**, 247–255 (2017).
- Al-Bassam, J. & Chang, F. Regulation of microtubule dynamics by TOG-domain proteins XMAP215/Dis1 and CLASP. *Trends Cell Biol.* **21**, 604–614 (2011).
- Cheeseman, I. M., Chappie, J. S., Wilson-Kubalek, E. M. & Desai, A. The conserved KMN network constitutes the core microtubule-binding site of the kinetochore. *Cell* **127**, 983–997 (2006).
- Chen, Y., Riley, D. J., Chen, P. L. & Lee, W. H. HEC, a novel nuclear protein rich in leucine heptad repeats specifically involved in mitosis. *Mol. Cell Biol.* **17**, 6049–6056 (1997).
- Wang, H.-W. et al. Architecture of the Dam1 kinetochore ring complex and implications for microtubule-driven assembly and force-coupling mechanisms. *Nat. Struct. Mol. Biol.* **14**, 721–726 (2007).
- Nabetani, A., Koujin, T., Tsutsumi, C., Haraguchi, T. & Hiraoka, Y. A conserved protein, Nuf2, is implicated in connecting the centromere to the spindle during chromosome segregation: a link between the kinetochore function and the spindle checkpoint. *Chromosoma* **110**, 322–334 (2001).
- Wigge, P. A. & Kilmartin, J. V. The Ndc80p Complex from *Saccharomyces cerevisiae* contains conserved centromere components and Has a function in chromosome segregation. *J. Cell Biol.* **152**, 349–360 (2001).
- Yamamoto, A. & Hiraoka, Y. Monopolar spindle attachment of sister chromatids is ensured by two distinct mechanisms at the first meiotic division in fission yeast. *EMBO J.* **22**, 2284–2296 (2003).
- Ding, D.-Q., Yamamoto, A., Haraguchi, T. & Hiraoka, Y. Dynamics of homologous chromosome pairing during meiotic prophase in fission yeast. *Dev. Cell* **6**, 329–341 (2004).
- Rothbauer, U. et al. A versatile nanotrapp for biochemical and functional studies with fluorescent fusion proteins. *Mol. Cell Proteom.* **7**, 282–289 (2008).
- Dodgson, J. et al. Spatial segregation of polarity factors into distinct cortical clusters is required for cell polarity control. *Nat. Commun.* **4**, 1834 (2013).
- Nithianantham, S. et al. Structural basis of tubulin recruitment and assembly by microtubule polymerases with tumor overexpressed gene (TOG) domain arrays. *eLife* **7**, e38922 (2018).
- Jumper, J. et al. Highly accurate protein structure prediction with AlphaFold. *Nature* **596**, 583–589 (2021).
- Varadi, M. et al. AlphaFold Protein Structure Database: massively expanding the structural coverage of protein-sequence space with high-accuracy models. *Nucleic Acids Res.* **50**, D439–D444 (2021).
- Hamada, T., Itoh, T. J., Hashimoto, T., Shimmen, T. & Sonobe, S. GTP is required for the microtubule catastrophe-inducing activity of MAP200, a tobacco homolog of XMAP215. *Plant Physiol.* **151**, 1823–1830 (2009).
- Farmer, V., Arpağ, G., Hall, S. L. & Zanic, M. XMAP215 promotes microtubule catastrophe by disrupting the growing microtubule end. *J. Cell Biol.* **220**, e202012144 (2021).
- Podolski, M., Mahamdeh, M. & Howard, J. Stu2, the budding yeast XMAP215/Dis1 homolog, promotes assembly of yeast microtubules by

- increasing growth rate and decreasing catastrophe frequency. *J. Biol. Chem.* **289**, 28087–28093 (2014).
51. Zahm, J. A., Stewart, M. G., Carrier, J. S., Harrison, S. C. & Miller, M. P. Structural basis of Stu2 recruitment to yeast kinetochores. *eLife* **10**, e65389 (2021).
 52. Tang, N. H., Takada, H., Hsu, K.-S. & Toda, T. The internal loop of fission yeast Ndc80 binds Alp7/TACC-Alp14/TOG and ensures proper chromosome attachment. *Mol. Biol. Cell* **24**, 1122–1133 (2013).
 53. Tang, N. H. & Toda, T. MAPping the Ndc80 loop in cancer: a possible link between Ndc80/Hec1 overproduction and cancer formation. *Bioessays* **37**, 248–256 (2015).
 54. Powers, A. F. et al. The Ndc80 kinetochore complex forms load-bearing attachments to dynamic microtubule tips via biased diffusion. *Cell* **136**, 865–875 (2009).
 55. Moreno, S., Klar, A. & Nurse, P. Molecular genetic analysis of fission yeast *Schizosaccharomyces pombe*. *Methods Enzymol.* **194**, 795–823 (1991).
 56. Bähler, J. et al. Heterologous modules for efficient and versatile PCR-based gene targeting in *Schizosaccharomyces pombe*. *Yeast* **14**, 943–951 (1998).
 57. Sato, M., Dhut, S. & Toda, T. New drug-resistant cassettes for gene disruption and epitope tagging in *Schizosaccharomyces pombe*. *Yeast* **22**, 583–591 (2005).
 58. Sato, M., Toya, M. & Toda, T. Visualization of fluorescence-tagged proteins in fission yeast: the analysis of mitotic spindle dynamics using GFP-tubulin under the native promoter. *Methods Mol. Biol.* **545**, 185–203 (2009).
 59. Ohta, M., Sato, M. & Yamamoto, M. Spindle pole body components are reorganized during fission yeast meiosis. *Mol. Biol. Cell* **23**, 1799–1811 (2012).
 60. Straight, A. F., Belmont, A. S., Robinett, C. C. & Murray, A. W. GFP tagging of budding yeast chromosomes reveals that protein–protein interactions can mediate sister chromatid cohesion. *Curr. Biol.* **6**, 1599–1608 (1996).
 61. Robinett, C. C. et al. In vivo localization of DNA sequences and visualization of large-scale chromatin organization using lac operator/repressor recognition. *J. Cell Biol.* **135**, 1685–1700 (1996).
 62. Shimada, T., Yamashita, A. & Yamamoto, M. The fission yeast meiotic regulator Mei2p forms a dot structure in the horse-tail nucleus in association with the *sme2* locus on chromosome II. *Mol. Biol. Cell* **14**, 2461–2469 (2003).
 63. Minagawa, M., Shirato, M., Toya, M. & Sato, M. Dual impact of a benzimidazole resistant β -tubulin on microtubule behavior in fission yeast. *Cells* **10**, 1042 (2021).
 64. Castoldi, M. & Popov, A. V. Purification of brain tubulin through two cycles of polymerization–depolymerization in a high-molarity buffer. *Protein Express. Purif.* **32**, 83–88 (2003).
 65. Hamada, T. et al. Stress granule formation is induced by a threshold temperature rather than a temperature difference in *Arabidopsis*. *J. Cell Sci.* **131**, jcs216051 (2018).
 66. Schindelin, J. et al. Fiji: an open-source platform for biological-image analysis. *Nat. Methods* **9**, 676–682 (2012).
 67. Meijering, E., Dzyubachyk, O. & Smal, I. Methods for cell and particle tracking. *Methods Enzymol.* **504**, 183–200 (2012).
 68. Bretz, F., Hothorn, T. & Westfall, P. *Multiple Comparisons Using R*. (CRC Press, 2010).
 69. Pettersen, E. F. et al. UCSF ChimeraX: structure visualization for researchers, educators, and developers. *Protein Sci.* **30**, 70–82 (2021).

Acknowledgements

We thank Ayumu Yamamoto, Yasushi Hiraoka, Takashi Toda and Masayuki Yamamoto for the yeast strains. We are grateful to Yuichiro Watanabe for microscopy support and to Yasutaka Kakui for valuable discussions. Y.M. was supported by JST SPRING, Grant no. JPMJSP2128. This study was supported by JSPS KAKENHI JP25291041, JP15H01359, JP16H04787, JP16H01317, JP18K19347, and JP21H00261 to M.S., and JP17K07397 and JP20K06645 to M.T. This study was also supported by the Ohsumi Frontier Science Foundation (OFSF), the Institute for Fermentation, Osaka (IFO) and Waseda University grants for Special Research Projects 2017B-242, 2017B-243, 2018B-222, 2019C-570, 2020R-038, and 2022C-164 to M.S and 2018S-139, 2019C-571, 2021C-584 and 2022C-170 to M.T.

Author contributions

Y.M. conducted yeast experiments supervised by M.S. and M.T., and in vitro experiments supervised by T.H., M.Y., and J.Y. T.H. designed the methodologies for the in vitro assays. N.O. contributed to material construction. M.S. conceived the outline of the study. Y.M. and M.S. wrote the paper with input from the co-authors.

Competing interests

The authors declare no competing interests.

Additional information

Supplementary information The online version contains supplementary material available at <https://doi.org/10.1038/s42003-022-04271-2>.

Correspondence and requests for materials should be addressed to Masamitsu Sato.

Peer review information *Communications Biology* thanks Robert Cross and the other, anonymous, reviewer(s) for their contribution to the peer review of this work. Primary Handling Editors: Patrick Meraldi and Eve Rogers.

Reprints and permission information is available at <http://www.nature.com/reprints>

Publisher's note Springer Nature remains neutral with regard to jurisdictional claims in published maps and institutional affiliations.



Open Access This article is licensed under a Creative Commons Attribution 4.0 International License, which permits use, sharing, adaptation, distribution and reproduction in any medium or format, as long as you give appropriate credit to the original author(s) and the source, provide a link to the Creative Commons license, and indicate if changes were made. The images or other third party material in this article are included in the article's Creative Commons license, unless indicated otherwise in a credit line to the material. If material is not included in the article's Creative Commons license and your intended use is not permitted by statutory regulation or exceeds the permitted use, you will need to obtain permission directly from the copyright holder. To view a copy of this license, visit <http://creativecommons.org/licenses/by/4.0/>.

© The Author(s) 2022